

The use of dense mixed ionic and electronic conducting membranes for chemical production

Alan Thursfield and Ian S. Metcalfe*

Department of Chemical Engineering, University of Manchester Institute of Science and Technology, PO Box 88, Manchester, UK M60 1QD. E-mail: i.metcalfe@umist.ac.uk

Received 15th April 2004, Accepted 18th June 2004
First published as an Advance Article on the web 21st July 2004

The exploitation of membranes within the chemical industry is an area of growing interest. Inorganic membranes promise high stabilities even under high temperature conditions (>200 °C). In addition, very high selectivities can be attained when dense ion-conducting membranes are employed. Here the characterisation of such dense inorganic membranes, through permeation studies, and the application of these membranes in chemical production are reviewed. Additional background information on membrane fabrication and techniques for characterisation is also provided.

1. Introduction

If membrane technologies are to be exploited, such membranes must be compatible with the desired temperature of operation of the membrane system. As many catalytic processes of industrial interest, such as hydrocarbon oxidation, hydrogenation and dehydrogenation reactions, proceed at temperatures above 200 to 300 °C, any membranes employed must be inorganic. Inorganic membranes can be broadly classified as being either dense or porous. All porous membranes suffer from problems relating to membrane selectivity, while dense membranes functioning as ion conductors can be tailored to exhibit a very high degree of selectivity yet still maintain reasonable conductivities at temperatures of interest.

All solids, to a greater or lesser extent, exhibit both ionic and electronic defects. Depending upon the concentration and mobility of these defects the material will exhibit ionic and electronic conduction. The conductivity of a species i , σ_i , can be related to the charge on the species z_i , the mobility, u_i , and the concentration of the species, C_i ,

$$\sigma_i = Fz_iu_iC_i \quad (1)$$

where F is Faraday's constant. The total conductivity, σ , of the material depends upon the sum of all individual conductivities,

$$\sigma = F \sum_i z_i u_i C_i \quad (2)$$

Hence individual conductivities can be expressed as a fraction of the total conductivity by using a transport number, t_i ,

$$\sigma_i = t_i \sigma \quad (3)$$

Here we will focus on materials that simultaneously exhibit both appreciable ionic conductivity and electronic conductivity, that is, mixed ionic and electronic conductors (MIECs). MIECs cannot be used for the direct external electrical control of the flux of a species to a catalyst surface nor can they be effectively employed in fuel cells. This limits their application to simultaneous reaction and separation problems. MIECs also

tend to be much better catalysts¹ than the catalytically inert solid electrolytes (ion transport number greater than 0.99) meaning that it may be possible in some applications to avoid the need for catalytic modification of the membrane surface. Indeed MIECs can be used as electrode materials²⁻⁴ because of their ability to conduct electrons coupled with their inherent catalytic activity. However, this catalytic activity and electronic conductivity also means that chemical stability can become an issue for these materials when exposed to a difference in oxygen chemical potential.

When used as a membrane, the MIEC essentially acts as a barrier between two chambers and only the ionically-conducted species can pass through the membrane under a chemical potential gradient. Such membranes promise advantages when used for oxidation processes as air can be used as an oxidant with no mixing of nitrogen with the product stream. This elimination of what is often a difficult separation can lead to process cost savings. Additionally, reaction selectivity may be improved in such systems as gas phase oxygen is no longer present on the reaction-side of the membrane. Fig. 1 shows a schematic representation of an oxygen-ion conducting MIEC membrane employed for the oxidation of a hydrocarbon.

It is the purpose of this paper to review the use of such MIEC membranes in chemical production. The vast majority of work in this area has been devoted to syngas (carbon monoxide and hydrogen) production from methane and natural gas and to a lesser extent the oxidative coupling of methane. Work on the former reaction system will be reviewed in detail (there has been very limited work with other reaction systems and such work will not be reviewed). Perhaps the most important consideration for an MIEC membrane used in chemical production is the transmembrane flux that it can deliver. For practical commercial use of oxygen-ion conductors an oxygen flux of 1 to 10 ml (STP) cm⁻² min⁻¹ has been suggested as necessary.^{5,6} This flux is intimately related to membrane performance and as a result this review article will also focus on the use of permeation studies in MIEC membrane characterisation and the relationship between such studies and membrane performance. For completeness we will also describe other techniques for membrane characterisation and indeed membrane fabrication including the selection of appropriate mixed-conducting

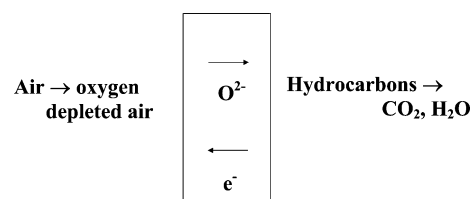


Fig. 1 Schematic of the function of a dense MIEC membrane supplying oxygen for hydrocarbon combustion.

materials where we will focus on the perovskite family. However, membrane characterisation and fabrication are not the focus of this review.

2. Mixed ionic–electronic conducting materials

Ion-conducting solid materials synthesised and studied thus far include, AgI, fluorite oxides, pyrochlore oxides, brownmillerite oxides, aurivillius oxides and ceramics based on the perovskite structure.⁷ The naturally occurring perovskite mineral is found enriched in cerium, niobium, thorium, lanthanum, neodymium and other rare earth metals. The mineral, CaTiO₃, has a cubic close-packed structure formed by the large O²⁻ and Ca²⁺ ions. Distortion of the cubic symmetry is possible and other symmetries such as rhombohedral may be encountered. The smaller Ti⁴⁺ cation occupies the centre of the cube and is octahedrally co-ordinated to the O²⁻ anions on the faces of the cube. The general formula is ABO₃ with the total charge of A and B equal to +6. The cubic structure is presented in Fig. 2. A perovskite without defects does not exhibit ionic conductivity. It is only when there are intrinsic defects present, or, defects are introduced, that it becomes a useful conductor that can be employed for applications of interest. The defects may take the form of vacancies at lattice sites, ions displaced into interstitial sites, impurities or lattice ions in a valence state such that A and B do not sum up to +6. In order for the lattice to remain electronically neutral, each charge defect must be compensated by another of equal magnitude and opposite sign. Doping with heterovalent cations is possible at both the A and B sites and can provide a number of complex perovskite families derived from the simple ABO₃ formula, for example, A_xA'_{1-x}B_yB'_{1-y}O_{3-δ} and A₃B'_{1+x}B''_{2-x}O_{9-δ} (a triple perovskite) with the A site in general occupied by large alkali earth metals and the B site by lanthanides and smaller first row transition elements (particularly important for an electronic contribution to the total conductivity). The creation of lattice oxygen vacancies is indicated by the 3-δ oxygen non-stoichiometry. The aim of the synthesis chemist is to dope heterovalent cations of similar size into the ABO₃ structure to create ionic and electronic conductivity and produce chemically and mechanically stable MIECs. The O²⁻ anion conductivity is achieved by doping-in acceptor cations of a lower charge than the cation they are replacing. The lower charge is compensated by O²⁻ vacancies, which at sufficiently high temperatures in an oxygen-containing atmosphere provide a vehicle for oxygen-ion conductivity through the lattice. While an increase in lattice oxide anion vacancies naturally leads to an increase in conductivity, too many vacancies will adversely affect the structure as the lattice becomes unstable resulting in more facile phase changes. The doping and resultant defect chemistry of the perovskite-based oxide-ion conductor is complex and the reader is directed to other sources that deal with this subject in detail.⁸⁻¹²

The aim of this review paper is to consider the application of

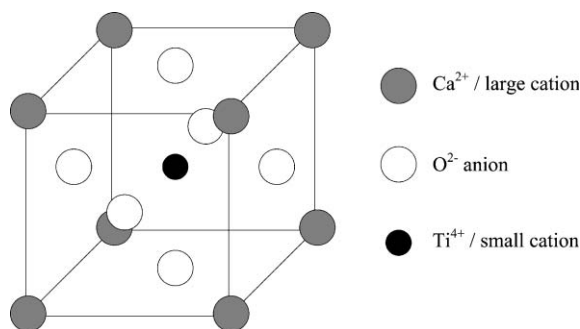


Fig. 2 The ideal cubic close packed ABO₃ perovskite structure.

these materials as membranes. In order for permeation of oxygen to take place through a ceramic membrane, adsorption and dissociation of oxygen molecules must occur on the surface at active adsorption sites. The adsorbed oxygen must be reduced and incorporated into the crystal lattice as oxide anions. Such surface processes can be grouped together and described by an oxygen surface exchange coefficient. Similar processes will also occur on the oxygen-evolving side of the membrane. The flux of oxygen, j_O , through the membrane surface can be expressed in terms of a partial pressure, chemical potential or concentration (gas phase or solid phase) driving force. Most commonly a solid-phase concentration driving force is used to obtain what is often termed a chemical surface exchange coefficient, k ,

$$j_O = k(C_{O,g} - C_O) \quad (4)$$

where C_O is the solid state oxygen concentration at the surface and the subscript g is used to denote a virtual solid state oxygen concentration that would be in equilibrium with the oxygen in the gas phase.

The MIEC membrane itself exhibits both ionic conductivity, σ_{ion} , and electronic conductivity, σ_e . The total membrane conductivity, σ , is given by the sum of the individual conductivities,

$$\sigma = \sigma_{ion} + \sigma_e \quad (5)$$

It can easily be shown that the current density of species i depends upon the charge on the species, its conductivity and the gradient in its electrochemical potential (where i is the electrochemical potential of the i th species),

$$i_i = -\frac{\sigma_i}{z_i F} \frac{d\bar{\mu}_i}{dx} \quad (6)$$

Therefore the ionic current can be described by,

$$i_{ion} = -\frac{\sigma_{ion}}{z_{ion} F} \frac{d\bar{\mu}_{ion}}{dx} \quad (7)$$

and the electronic current, if carried by electrons (n-type conductor),

$$i_e = \frac{\sigma_e}{F} \frac{d\bar{\mu}_e}{dx} \quad (8)$$

In the absence of an external electrical circuit,

$$i_{ion} + i_e = 0 \quad (9)$$

and therefore,

$$\frac{\sigma_{ion}}{z_{ion} F} \frac{d\bar{\mu}_{ion}}{dx} = \frac{\sigma_e}{F} \frac{d\bar{\mu}_e}{dx} \quad (10)$$

In oxygen deficient perovskites (general formula of ABO_{3-δ}) the ion flux is carried by oxygen-ion vacancies and we may write the above in terms of oxygen vacancy conductivity, σ_V , and electrochemical potential, $\bar{\mu}_V$,

$$\frac{\sigma_V}{2F} \frac{d\bar{\mu}_V}{dx} = \frac{\sigma_e}{F} \frac{d\bar{\mu}_e}{dx} \quad (11)$$

and the flux of vacancies can be evaluated from,

$$j_V = \frac{i_V}{2F} = -\frac{\sigma_V}{4F^2} \frac{d\bar{\mu}_V}{dx} \quad (12)$$

where,

$$\sigma_V = \frac{D_V}{RT} 4F^2 C_V, \text{ or, } j_V = -\frac{D_V C_V}{RT} \frac{d\bar{\mu}_V}{dx} \quad (13)$$

and D_V is the diffusion coefficient of oxygen-ion vacancies and C_V is the concentration of these vacancies.

Alternatively the flux may be expressed in terms of an oxygen

diffusion coefficient, D_O , in which case it can be shown that,

$$D_V C_V = D_O C_O \quad (14)$$

where C_O is the lattice oxygen concentration. The concentration of vacancies and occupied oxygen lattice sites can be related to the total site concentration, C , using the degree of non-stoichiometry, δ ,

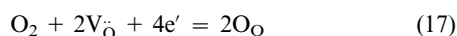
$$C_V = \frac{\delta}{3} C \text{ and } C_O = \left(\frac{3-\delta}{3}\right) C \quad (15)$$

and hence,

$$D_V \left(\frac{\delta}{3-\delta}\right) = D_O \quad (16)$$

The degree of non-stoichiometry is often small (between 0 and 0.1) and therefore oxygen diffusion coefficients tend to be much smaller than vacancy diffusion coefficients.

Defect concentrations are determined by reaction between gas-phase oxygen, oxygen vacancies and electrons on both sides of the membrane through the reaction,



The oxygen chemical potential difference across the membrane results in an electrochemical potential difference in oxygen-ion vacancies and electrons such that, in the absence of surface limitations,

$$\begin{aligned} \Delta\mu_{\text{O}_2} &= 2\Delta\mu_{\text{O}} = -2\Delta\bar{\mu}_V - 4\Delta\bar{\mu}_e, \text{ or,} \\ d\mu_{\text{O}_2} &= 2d\mu_{\text{O}} = -2d\bar{\mu}_V - 4d\bar{\mu}_e \end{aligned} \quad (18)$$

Combining with Equation (11), we obtain,

$$d\bar{\mu}_V = -\frac{1}{2} \frac{\sigma_e}{\sigma} d\mu_{\text{O}_2} \quad (19)$$

and therefore, using Equation (12),

$$j_V = \frac{1}{8F^2} \frac{\sigma_V \sigma_e}{\sigma} \frac{d\mu_{\text{O}_2}}{dx} \quad (20)$$

To proceed, we assume that the electron transfer number approaches unity and therefore there is no gradient in electrical potential in the membrane. Substituting for electrochemical oxygen potential in terms of oxygen partial pressure in the absence of a gradient in electrical potential gives,

$$j_V = \frac{RT}{8F^2} \sigma_V \frac{d \ln P_{\text{O}_2}}{dx} = \frac{1}{2} D_V C_V \frac{d \ln P_{\text{O}_2}}{dx} \quad (21)$$

or

$$j_V = -\frac{RT}{4F^2} \frac{\sigma_V}{C_V} \gamma \frac{dC_V}{dx} = -D_V \gamma \frac{dC_V}{dx} \quad (22)$$

where γ is known as the thermodynamic factor and is given by,

$$\gamma = -\frac{1}{2} \frac{d \ln P_{\text{O}_2}}{d \ln C_V} \quad (23)$$

(The thermodynamic factor is used to convert between thermodynamic diffusion coefficients (electrochemical potential driving force) and diffusion coefficients based on a concentration driving force.)

Permeation experiments performed on the membrane in the absence of surface limitations determine a chemical diffusion coefficient, \tilde{D} ,

$$j_V = -\tilde{D} \frac{dC_V}{dx} \quad (24)$$

Such experiments require the integration of Equation (24). Most commonly, under the conditions of operation, the

chemical diffusion coefficient is assumed to be independent of membrane depth and the limits of vacancy concentration are determined from data on the degree of non-stoichiometry of the material *versus* oxygen partial pressure or chemical potential. Comparing Equations (22) and (24), the chemical diffusion coefficient can easily be related to the vacancy diffusion coefficient,

$$\tilde{D} = \gamma D_V \quad (25)$$

and the thermodynamic factor and can be evaluated from the degree of oxide non-stoichiometry *versus* oxygen partial pressure or chemical potential.

Ideally, for an n-type oxygen-deficient perovskite, γ is given by¹³

$$\gamma = -\frac{1}{2} \frac{d \ln P_{\text{O}_2}}{d \ln C_V} = 3 \quad (26)$$

and the chemical diffusion coefficient obtained in such experiments is easily related to the vacancy diffusion coefficient and the oxygen diffusion coefficient,

$$\tilde{D} = 3D_V = 3 \left(\frac{3-\delta}{\delta}\right) D_O \quad (27)$$

This means that to practically determine diffusion coefficients, the conditions under which the membrane is operated must be known along with information on membrane thickness, oxygen flux and degree of non-stoichiometry as a function of oxygen partial pressure or chemical potential.

3. Membrane fabrication and characterisation

3.1. Ceramic powder synthesis

The perovskite oxides can be synthesised by a number of different routes that can be categorised according to whether they involve solid-state reaction, gel formation or solution or vapour phase processes.

Solid-state reaction is perhaps the most common and most direct method used because of its simplicity. High purity oxides or carbonates (>99%) of the component elements in cationic form are thoroughly mixed together by ball milling for around 24 hours in order to obtain a homogeneous powder. The powder is then heated to in excess of 1000 °C to facilitate the solid-state reaction of the oxides. The process may be repeated several times. Often, the resultant powder is sieved to the required particle size.

The sol-gel method was developed in the 1950's for the production of radioactive powders of UO₂ and ThO₂ for nuclear fuels without generation of large quantities of dust. The method involves the production of gels from liquids followed by calcining to form the product. Sols are dispersions of solid particles with at least one dimension between 1 nm and 1 μm in a continuous liquid. Gels consist of a continuous solid skeleton enclosing a continuous liquid so that producing a gel from a sol requires linking the solid phase in the system. This is a more involved and expensive synthesis route than the solid-state reaction. Metal nitrates or alkoxides of the constituent elements of the ceramic are dissolved in water and a chelating agent is added. The mixture is heated and stirred causing polymerisation, followed by condensation. Evaporation of the water causes the gel to form, which is then heated to remove the organics, leaving the ceramic powder product.

Co-precipitation is one of the oldest methods of preparing mixed oxides. An aqueous solution of the metal cations is mixed with another solution that contains a precipitating agent. The precipitated product is filtered, dried and thermally decomposed to isolate the ceramic powder. Care must be taken to ensure that parameters such as pH, temperature, concentration and mixing rates are optimised. Different rates of

precipitation of each component may lead to inhomogeneity. Precipitation of the metal hydroxides with metal nitrates, chlorides and oxalates, dissolved in an acidic aqueous solution, can yield high purity powders of small particle size.

Spray drying involves the rapid vaporisation of a solution of the metal cations. Freeze drying involves spraying of fine droplets into liquid nitrogen followed by slow sublimation of the solvent. These methods enable one to control impurities and produce fine homogeneous particles, in some cases as small as 10 nm.

In solid state combustion (SSC) there are two modes; self-propagating high temperature synthesis (SHS) and volume combustion synthesis (VCS). The reactants are mixed, pelleted and ignited by an external source. The combustion wave passes through the heterogeneous mixture yielding the condensed ceramic phase. The method can be used in conjunction with applied electromagnetic fields (field activated combustion synthesis, FACS). Another development is solution combustion (SC) that has been used to prepare a wide range of metal oxides and found to be particularly efficient at doping metals into oxides. Spray pyrolysis employs a solution of the appropriate metal nitrates, at the required stoichiometry, which is fed into a nebuliser. The nebuliser produces a fine spray of the metal nitrates that passes into a reaction chamber maintained at around 800 °C. The reaction produces a particularly fine ceramic powder.

Other methods applied to solid oxide synthesis include hydrothermal methods, plasma spraying, electron beam evaporation and arc vaporisation. The interested reader is directed to reviews on metal oxide synthesis such as those by Cousin and Ross¹⁴ and Patel *et al.*¹⁵

3.2. Powder characterisation

The quality and performance of the ceramic powder must be quantified. There are many techniques now available to aid the material scientist in doing this. Below we describe briefly some of the more common methods that are routinely employed.

X-Ray diffraction is essential in determining crystallinity and phase purity of the ceramic powder. It is also often used in post-operation studies where the material has for example been used in demanding environments that could have had adverse effects on the crystal structure. The method has also been used for *in situ* studies of crystal growth in oxide systems. Scanning electron microscopy (SEM) and transmission electron microscopy (TEM) are used to determine particle size (among a range of other techniques) and morphology of the ceramic powder. During thermogravimetric analysis (TGA) the sample temperature is increased with time and the weight of the ceramic powder is monitored. The weight loss at a specific temperature and oxygen partial pressure corresponds to the creation of lattice oxygen vacancies and reduction of metal cations. This technique can be used to determine the degree of non-stoichiometry of the oxide *versus* oxygen partial pressure or chemical potential.

Solid state nuclear magnetic resonance (NMR) is not commonly used with ceramic powders due to cost of the technique and the difficulty in studying many nuclei of interest. The technique is more easily applied to systems with spin ½ nuclei such as ¹H and ²⁹Si. However the quadrupolar nature of many of the elements in metal oxides, including ¹⁷O itself, adds complications but useful data can be obtained even with these difficult nuclei. The NMR parameters; T_1 (longitudinal) and T_2 (transverse) relaxation measurements of ¹⁷O have been used to determine the chemical diffusion coefficient, \bar{D} .¹⁶ High temperature ¹⁷O NMR has been used, in conjunction with high temperature XRD, to investigate structural changes in metal oxides and to observe oxygen vacancies. Most studies have used ¹⁷O but other nuclei studied include ¹³⁹La.

A comprehensive survey of analytical techniques employed

for ceramic powder characterisation dealing with issues such as phase state and structure, size, shape, strain and microstructure is provided elsewhere.¹⁷

3.3. From ceramic powder to dense membrane

The ceramic powder once synthesised and characterised needs to be processed into a form appropriate for the application under consideration. Traditional ceramic membrane forming processes have included, die pressing, cold isostatic pressing, slip casting and extrusion. More recently methods such as injection moulding and tape casting have been developed. Some traditional methods have been developed further to meet particular property requirements resulting in new methods such as hot pressing, hot isostatic pressing and pressure casting. As the synthesis chemist must endeavour to produce high quality well-characterised ion-conducting ceramics, so the process technologist must ensure that membranes fabricated from these ceramic powders are of a high standard to minimise flaws and defects. The three basic shaping processes for ceramics powders are pressing, casting and plastic forming.

Die pressing is the most widely used shaping technique for laboratory scale studies such as oxygen permeation and conductivity tests and consists of the uniaxial compaction of a ceramic powder while confined in a compression die. Applied pressure is of the order of 200–500 MPa with disk size typically 10 to 20 mm in diameter and 1 to 2 mm in thickness depending on die size and the quantity of ceramic powder used. During isostatic pressing the powder, or preformed die-pressed compact, is loaded into a flexible air-tight container, typically polyurethane, placed in a closed pressure vessel filled with liquid and compacted by increasing the pressure within the vessel. The pressure change takes place throughout the liquid, thus exerting a uniform applied pressure over the entire surface area of the airtight container. In this way, the material is uniformly compacted and will retain the general shape of the flexible container. In hot isostatic pressing a compact is sintered at high temperature in a pressurised gas atmosphere. The compact must either be impermeable to the pressurising gas or be encapsulated in a gas-tight container. In the former case, powder compacts are first sintered to remove surface connected porosity. The use of hot isostatic pressing leads to additional densification and increased strength.

In slip casting, a “slip”, consisting of a low viscosity suspension of micrometer size ceramic particles in a liquid (usually water), is poured into a porous mould. The mould absorbs some of the liquid from the outer layers of the suspension, which is then inverted and the remaining suspension is poured out to make hollow objects as in slush casting of metals. For solid ceramic objects, the slip is supplied continuously into the mould to replenish the absorbed water. The suspension is not drained from the mould but is left as a soft solid referred to as the “green”, as in powder metallurgy. Tape casting (also known as “doctor blading” and “knife coating”) facilitates the production of sheets of ceramic from 5 µm to 1 mm in thickness. A slip is used which is poured onto a rolling film. The process utilises a scraping blade, known as the “doctor” for the removal of excess slip material from a moving surface (similar to a conveyer belt) that is being coated. Alternatively the surface can be stationary and the doctor blade traversed along the length of the surface that supports the slip.

The extrusion processes consist of forcing a plastic mix of a ceramic powder through a constricting die to produce elongated shapes that have a constant cross-section. The slip consists of a fine ceramic powder with the appropriate addition of binder(s) and plasticiser(s) to give the desired flow properties either cold, or when heated, prior to being forced through the die. Low pressure injection moulding (LPIM) has several major benefits over more traditional manufacturing techniques such as die pressing. It is a good technique for high volume

components and provides an option for producing ceramic components using low cost tools in comparison to high pressure moulding techniques. The LPIM process enables fabrication of very complex shapes as well as simpler components.

After the shape-forming process the membrane undergoes a sintering process. Sintering the membrane to temperatures in the range 500 to 1500 °C (depending on the specific ceramic and method of fabrication) causes densification to take place as surface reactions between the crystallites (or "grains") that comprise the membrane structure take place. The crystals bond to their neighbours and in so doing eliminate the void spaces between. This process also gives rise to the phenomenon of "grain boundaries".¹⁸ Such grain boundaries can have a positive or negative effect on the ionic and electronic conductivity of the membrane but are an unavoidable complication once sintering has occurred. The study of grain boundaries is outside of the scope of this review and will not be considered further.

For applications of the membrane, a number of reactor configurations exist; the membrane can take the form of a disk/pellet or a tube that can be either open-ended or sealed at one end. The most used membrane design in MIEC studies has tended to be the simple disk. However, a recent paper by Trunec has shown that good quality dense thin walled tubes of around 10 mm in diameter with a wall thickness of around 300 µm can be made.¹⁹ The idea of the tubular reactor has recently been taken a step further by Liu *et al.*^{20–22} and Luyten *et al.*²³ In their work they were able to make dense fine hollow fibres of a number of ceramic materials by spinning a dope comprising the ceramic powder in a polymer binder. Presented in Fig. 3 is an SEM of the cross section of a typical hollow fibre, inner diameter values are of the order of 1 mm and length *ca.* 200 mm. When used in bundles such designs can address the problem, at laboratory scale, of low reactor surface area and provide a high throughput of pure oxygen for high product yields. The reader is directed to a number of review articles dealing with the use of dense oxide-ion conducting membranes focusing on aspects such as membrane material selection, reactor design and chemical process applications.^{24–26}

3.4. Membrane characterisation

Characterisation of the membranes falls into three general classifications. Firstly, techniques may be used to investigate the physical nature of the membrane. Imaging can readily give the grain size distribution and show the grain boundaries. Imaging of the membrane surface can also indicate imperfections such as cavities and porosity and estimate relevant surface areas.

Secondly, specific methods can be used to measure individual diffusion coefficients and surface exchange coefficients by relying upon the differing length-scales involved in, or the differing inherent time constants of, the relevant processes (the implementation of such techniques can be quite complex and

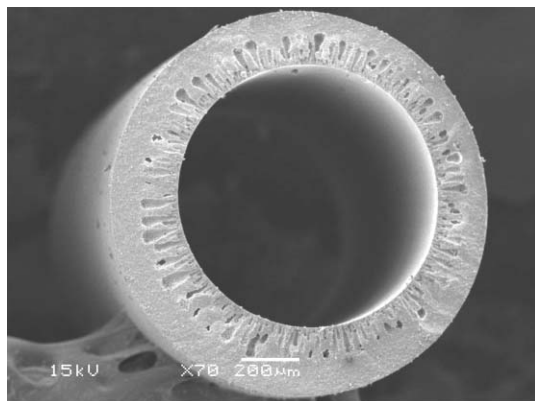


Fig. 3 SEM cross-section of a dense ceramic hollow fibre filament.

will not be covered here). Surface exchange coefficients and tracer diffusion coefficients (related to thermodynamic diffusion coefficients) can be separated using oxygen diffusion measurements methods. In the ¹⁶O–¹⁸O isotope tracer method coupled with secondary ion mass spectroscopy (SIMS), the membrane sample is heated in natural abundance oxygen and then cooled. Following evacuation, ¹⁸O₂ is introduced and the sample heated to the same temperature as was used for natural abundance O₂. The sample is then sectioned and the ¹⁸O diffusion profile measured by SIMS line-scanning.²⁷ The tracer diffusion coefficient and surface exchange coefficient can be determined by fitting the isotopic fraction of oxygen to the solution for the one dimensional diffusion equation for semi-infinite media. The oxygen tracer diffusion coefficient is equal to the oxygen diffusion coefficient divided by the Haven ratio. The Haven ratio accounts for correlation effects in tracer diffusion.¹³ The surface exchange coefficient is sensitive to the condition of the surface of the membrane sample and encompasses a number of surface processes such as adsorption, disassociation *etc.* These factors make agreement of values for surface exchange coefficients for a given sample difficult and there is often disagreement in the literature. AC impedance spectroscopy (IS), or, electrical impedance spectroscopy (EIS) can be used to separate the resistances associated with a membrane as a result of their different time constants. A small AC electrical field is applied to the membrane over a frequency range of, *e.g.*, 10⁶ to 0.1 Hz. Each process occurring within the membrane has a characteristic response and grain boundary resistances can even be separated from bulk resistances. Conductivities are then easily calculated from individual resistances. Application of IS to MIECs requires the use of so-called blocking electrodes, *i.e.*, a material sandwiched between the MIEC membrane and current collector that excludes one of the current contributions. An example of this is the use of the pure oxide anion conductor YSZ deposited on an MIEC membrane with a Pt electrode in turn deposited on the YSZ layer. In this configuration the YSZ only allows the ionic contribution from the total current passing through the MIEC to be collected at the Pt electrode. To block the ionic contribution in MIECs, plates of inert metal or graphite can be used. Conductivity relaxation experiments involve changing the oxygen partial pressure surrounding a sample and monitoring the change in electrical conductivity *versus* time. Provided that the ionic conductivity of the sample is much less than its electronic conductivity, the relaxation is controlled by the movement of ionic species. Solution of the governing equations results in a model that can be compared to the transient conductivity data to yield a chemical diffusion coefficient and surface exchange coefficient.

Finally, the most common approach to membrane characterisation involves studying oxygen permeation. Such an approach yields information about overall transport rates and it can, therefore, be difficult to assign a rate-determining step or determine exchange and diffusion coefficients. In the permeation experiment the membrane separates two compartments within a sealed cell. On one side of the membrane an inert, often helium, is introduced at a given flow rate while on the other side oxygen is introduced at a known flow rate and partial pressure. (It should be noted that the oxygen flux through the membrane will result in an oxygen chemical potential on the helium side. It could be argued that such experiments would be better conducted by introducing a fixed oxygen chemical potential, albeit a low oxygen chemical potential, on this side of the membrane. However, not all experiments reviewed were conducted with a fixed oxygen chemical potential on the anodic side.) At elevated temperatures oxygen permeates through the membrane under the oxygen chemical potential gradient and enters the inert gas stream. The inert and oxygen permeate leave the cell and are

Table 1 MIECs investigated for oxygen permeation and syngas production

Perovskite type	CMR configuration(s)	Investigation(s) and references	Catalysts used in conjunction with membrane
La _{0.6} Sr _{0.4} Co _{0.2} Fe _{0.8} O _{3-δ}	disk:tubular	O ₂ ²⁸⁻³¹ :CO + H ₂ ^{56,57,67}	Ni/Al ₂ O ₃ ^{56,57} Ni ⁶⁷
La _{0.6} Sr _{0.4} Co _{0.8} Fe _{0.2} O _{3-δ}	disk	O ₂ ³³ :CO + H ₂ ⁵⁸	none ⁵⁸
La _{0.6} Sr _{0.4} Co _{0.6} Fe _{0.4} O _{3-δ}	disk	O ₂ ³⁴	none
La _{0.2} Sr _{0.8} Co _{0.8} Fe _{0.2} O _{3-δ}	disk:tubular	O ₂ ³³ :CO + H ₂ ⁵⁹	Rh-based ⁵⁹
La _{0.2} A _{0.8} Co _{0.2} Fe _{0.8} O _{3-δ} (A = Sr, Ba, Ca)	disk	O ₂ ³²	none
La _{0.1} Sr _{0.9} Co _{0.9} Fe _{0.1} O _{3-δ}	disk	O ₂ ³³	none
La _{0.4} Ca _{0.6} Co _x Fe _{1-x} O _{3-δ} (x = 0, 0.25, 0.5)	disk	O ₂ ³⁷	none
La _{0.2} Sr _{0.8} Cr _{0.2} Fe _{0.8} O _{3-δ}	disk and tubular	O ₂ ⁶⁰⁻⁶³	none
La _{0.7} Sr _{0.3} Ga _{0.6} Fe _{0.4} O _{3-δ}	disk	O ₂ ⁶⁶ :CO + H ₂ ⁶⁶	Ni, Pd, Ru, Rh, Co, Fe ⁶⁶
La _{0.8} Sr _{0.2} Ga _{0.7} M _{0.3} O _{3-δ} (M = Fe, Co, Ni)	disk	O ₂ ⁶⁶ :CO + H ₂ ⁶⁷	Ni ⁶⁷
La _{0.8} Sr _{0.2} Ga _{0.8} Mg _{0.2-x} Co _x O _{3-δ} (x = 0 to 0.2)	disk	O ₂ ³⁸	none
La _{0.9} Sr _{0.1} Ga _{0.65} Mg _{0.15} Ni _{0.2} O _{3-δ}	disk	O ₂ ³⁹	none
La _{0.5} Pr _{0.5} Ga _{0.65} Mg _{0.15} Ni _{0.2} O _{3-δ}	disk	O ₂ ³⁹	none
La _{1-x} Sr _x FeO _{3-δ} (x = 0.1 to 0.4)	disk	O ₂ ³⁶	Pt ³⁶
SrCo _{0.8} Fe _{0.2} O _{3-δ}	disk and tubular : tubular	O ₂ ^{33,40} :CO + H ₂ ⁶⁴	Rh-based ⁶⁴
SmFe _{0.5} Co _{0.5} O _{3-δ}	tubular	O ₂ ⁴⁰	none
Sr _{0.25} Bi _{0.5} FeO _{3-δ}	disk	O ₂ ⁴¹	none
YSZ-SrCo _{0.4} Fe _{0.6} O _{3-δ}	tubular	CO + H ₂ ⁶⁵	Ni/Al ₂ O ₃ ⁶⁵
SrCo _{0.4} Fe _{0.6-x} Zr _x O _{3-δ} (0 ≤ x ≤ 0.2)	disk	O ₂ ⁴²	none
SrCo _{0.95-x} Fe _x Zr _{0.05} O _{3-δ} (0.1 ≤ x ≤ 0.8)	disk	O ₂ ⁴²	none
BaBi _x Co _{0.2} Fe _{0.8-x} O _{3-δ} (0.1 ≤ x ≤ 0.5)	disk	O ₂ ⁴³	none
Ba _{0.5} Sr _{0.5} Co _{0.8} Fe _{0.2} O _{3-δ}	disk and tubular : disk and tubular	O ₂ ^{44,45} :CO + H ₂ ^{53,68-70}	LiLaNiO/Al ₂ O ₃ ⁶⁸⁻⁷⁰
{La _{0.15} Sr _{0.85} Ga _{0.3} Fe _{0.7} O _{3-δ} Ba _{0.5} Sr _{0.5} Co _{0.8} Fe _{0.2} O _{3-δ} }	disk (dual phase)	O ₂ ⁴⁶	none

^a O₂: oxygen flux/stability/conductivity study. ^b CO+H₂: syngas production study.

analysed by, *e.g.*, gas chromatography and/or mass spectroscopy. Here we include recent oxygen permeation studies on perovskite materials in this review, see Table 1. (When volumetric oxygen permeation fluxes have been reported in the literature at standard temperature and pressure (STP) we have quoted these values. However, in a number of articles, there is no mention of the conditions under which the volumetric flux was calculated. For these articles we report the volumetric flux as quoted but we omit referring to STP.) When we quote only one flux we have attempted to use the maximum flux obtained in the study or the most stable one obtained. Under conditions of maximum flux we also quote membrane thickness, temperature and oxygen partial pressures used for the permeation driving force. All studies reported were performed at atmospheric pressure. It is common practise to abbreviate the chemical formula of complex perovskites by using the first letter of the chemical symbol of each of the constituent elements, *e.g.*, "L" for La, "S" for Sr, but often oxygen is omitted from the list of symbols. This string of letters is then followed by a string of digits each of which corresponds to the stoichiometry of the corresponding letter (we use the full chemical formula and the abbreviated formula interchangeably).

The doped lanthanum cobaltite families have attracted great attention with particular interest in the chemically and mechanically robust La_{0.6}Sr_{0.4}Co_{0.2}Fe_{0.8}O_{3-δ} (LSCF6428) because of its good ionic and electronic conductivity. Studies such as that by Lane *et al.*²⁸ have focused on important aspects such as ionic conductivity, oxygen diffusion and oxygen surface exchange as a function of temperature and oxygen partial pressure. They used a disk membrane configuration, of thickness 0.96 mm, and techniques such as electrical conductivity relaxation, TGA and ¹⁸O tracer coupled with SIMS. An oxygen flux of around 0.04 ml cm⁻² min⁻¹ was obtained at 800 °C using helium (containing 0.001 atm of oxygen) and air on either side of the disk. An oxygen partial pressure range of 0.03 to 1 atm was used for the determination of diffusion coefficients and surface exchange coefficients employing the ¹⁸O tracer method and conductivity relaxation. Using the ¹⁸O tracer method values for the tracer diffusion coefficient were determined to be in the range of *ca.* 10⁻⁷ to *ca.* 10⁻⁸ cm² s⁻¹. Chemical diffusion coefficients were determined by conductivity relaxation to be between *ca.* 3 × 10⁻⁶ and *ca.* 10⁻⁵ cm² s⁻¹.

Using the Haven ratio and appropriate thermodynamic factor the two diffusion coefficients were found to be in good agreement. Surface exchange coefficients determined by the two techniques, however, did not show good agreement and the authors recommended further work. Permeation studies²⁹ on a tubular membrane design of thickness 1.5 mm fabricated by plastic extrusion gave oxygen fluxes up to 0.13 ml (STP) cm⁻² min⁻¹ (0.1 μmol cm⁻² s⁻¹) at 900 °C using helium (containing 0.001 atm of oxygen) and air on either side of the tube. An overall oxygen permeation activation energy of 168 kJ mol⁻¹ was calculated. During the study evidence of deterioration of the material due to contamination with traces of SO₂ in the air leading to SrO₄, CoSO₄, SrO, CoO and La₂O₃ was found. The study did not include experiments to separate surface exchange or bulk diffusion kinetics. The same group have more recently looked into the possibility of using a LSCF6428 disk as a support for a thick porous coating of the same perovskite to make an asymmetric membrane.³⁰ A slurry of LSCF6428 was first prepared and then deposited onto the support of thickness 1 to 2 mm by slip casting with subsequent sintering. This configuration provided oxygen fluxes from 600 to 800 °C of 0.1 ml (STP) cm⁻² min⁻¹ to 0.2 ml (STP) cm⁻² min⁻¹ (0.07 μmol cm⁻² s⁻¹ to 0.14 μmol cm⁻² s⁻¹) using helium and atmospheric air on either side of the disk. These fluxes were three times that obtained for the dense support disk alone. The higher flux in the asymmetric membrane was attributed to a lowering of the overall oxygen permeation activation energy but no reason for this lower activation energy was given. An overall activation energy for oxygen permeation was calculated as 18 kJ mol⁻¹ compared to *ca.* 160 kJ mol⁻¹ as is commonly reported for this material. Using AC IS Diethelm and Van herle³¹ determined the chemical diffusion coefficient of 1.7 × 10⁻⁵ cm² s⁻¹ and a surface exchange coefficient (based on a solid-state concentration driving force) of 3.6 × 10⁻⁴ cm s⁻¹ in air at 900 °C for disks of LSCF6428. With a disk membrane of thickness 1.53 mm a permeation flux of 0.08 μmol cm⁻² s⁻¹ was measured using argon and air on either side of the disk. They found that permeation was under control of both bulk diffusion and surface exchange.

Other stoichiometries of perovskites based on LSCF have been investigated. The La_{0.2}A_{0.8}Co_{0.2}Fe_{0.8}O_{3-δ} (A = Sr, Ba, Ca) series was investigated using a disk membrane configuration

with helium and atmospheric air on either side of the disk.³² It was found that the oxygen flux was highest with the strontium-substituted perovskite because of its low average bond strength, high free volume and large critical volume. However, at high temperature and in low oxygen partial pressures the material decomposed to La_2O_3 , SrO , cobalt and iron. In comparison the barium-substituted material was found to be more stable under these conditions. The overall oxygen permeation activation energies for A = Sr, Ba and Ca were calculated as 106, 123 and 144 kJ mol^{-1} respectively at 900 °C. The chemical diffusion coefficients were calculated to be 17.1, 8.54, $2.85 \times 10^{-6} \text{ cm}^2 \text{ s}^{-1}$ for the Sr-, Ba- and Ca-substituted oxide. The steady state values for the oxygen permeation fluxes in the Sr-, Ba- and Ca-substituted oxides were 0.81 $\text{ml (STP) cm}^{-2} \text{ min}^{-1}$ ($0.63 \mu\text{mol cm}^{-2} \text{ s}^{-1}$), 0.40 $\text{ml (STP) cm}^{-2} \text{ min}^{-1}$ ($0.29 \mu\text{mol cm}^{-2} \text{ s}^{-1}$) and 0.12 $\text{ml (STP) cm}^{-2} \text{ min}^{-1}$ ($0.09 \mu\text{mol cm}^{-2} \text{ s}^{-1}$) respectively at 950 °C using membranes of thickness 2 mm for the Sr- and Ba- substituted oxides and 1 mm for the Ca-substituted oxide. In the case of the Ca-substituted oxide a very similar flux ($0.09 \mu\text{mol cm}^{-2} \text{ s}^{-1}$) is seen for a similar temperature and membrane thickness to those used in the work of Diethelm and Van herle³¹ on LSCF6428 ($0.08 \mu\text{mol cm}^{-2} \text{ s}^{-1}$). However the chemical diffusion coefficients are significantly different ($2.85 \times 10^{-6} \text{ cm}^2 \text{ s}^{-1}$ versus $1.7 \times 10^{-5} \text{ cm}^2 \text{ s}^{-1}$). This does not necessarily mean that vacancy diffusion coefficients were very different in the two cases as a difference in vacancy concentration could explain the difference in the chemical diffusion coefficients. However given the different nature of the data presented regarding the degree of non-stoichiometry in the two cases (TGA versus thermodynamic factors) a direct comparison is difficult to make.

Studies on LSCF powder coatings on LSCF membrane disks were undertaken by Teraoka *et al.*³³ using LSCF1991, LSCF2882 and LSCF6482 and also $\text{SrCo}_{0.8}\text{Fe}_{0.2}\text{O}_{3-\delta}$ disks coated with porous coatings of LaCoO_3 , $\text{La}_{0.8}\text{Sr}_{0.2}\text{CoO}_{3-\delta}$ and $\text{SrCo}_{0.8}\text{Fe}_{0.2}\text{O}_{3-\delta}$ perovskites of approximately 150 μm thickness. The difference in the oxygen sorption-desorption capacity of the coating and the disk influenced oxygen permeation when the coating was used as a cathode material. As anodic coatings, for oxygen evolution, the effect of the coating was simply to increase the surface area of the disk. Oxygen permeation values ranging from 0.2 to 2.0 $\text{ml (STP) cm}^{-2} \text{ min}^{-1}$ (0.14 to $1.48 \mu\text{mol cm}^{-2} \text{ s}^{-1}$) were observed at 900 °C on disks of thickness 1 mm using helium and synthetic air on either side of the disk. A thorough study of the transport parameters of LSCF6464 has been carried out by ten Elshof *et al.*³⁴ using electrical conductivity relaxation and high temperature coulometric titration techniques in the temperature range 650 to 980 °C under 0.03 to 1 atm of oxygen with nitrogen as diluent. The chemical diffusion coefficient was in the range of 10^{-6} to $5 \times 10^{-5} \text{ cm}^2 \text{ s}^{-1}$ with an activation energy in the range of 90 to 120 kJ mol^{-1} . The authors noted that the surface exchange coefficients (from 10^{-6} to $10^{-2} \text{ cm s}^{-1}$ based on a solid-state concentration driving force) were dependent on oxygen partial pressure and concluded that the rate-determining step in the surface exchange process involved molecular oxygen. However, it should be noted that mass transfer control could explain the dependence: mass transfer could possibly have been ruled out as the controlling process in error. Fixed-bed reactors packed with powders of LSCF1955 and LSCF1991 that adsorb particularly large quantities of oxygen due to their high Sr content, have shown promise as systems for a new oxygen sorption process for oxygen/nitrogen separation and may prove to be good candidates for membrane reactor processes.³⁵

Studies on other La-containing perovskites have included disks of $\text{La}_{1-x}\text{Sr}_x\text{FeO}_{3-\delta}$ ($x = 0.1$ to 0.4) in the temperature range 850 to 1050 °C.³⁶ It was discovered that treatment of the lower oxygen partial pressure side with a CO-containing

atmosphere (carbon monoxide partial pressures ranging from 0 to 0.3 atm) at high temperature led to improved oxygen fluxes of up to $2.5 \mu\text{mol cm}^{-2} \text{ s}^{-1}$ possibly as a result of enlargement of the membrane surface area arising from segregation of the perovskite into SrCO_3 and SrO at the surface. Surface modification of the $x = 0.2$ perovskite, sputter coated with a 50 nm layer of platinum, increased the permeation rate by a factor of *ca.* 1.8 indicating surface exchange control of the permeation. Experiments in which membranes of thicknesses between 0.5 to 2 mm were used with helium containing between 0.001 and 0.02 atm of oxygen, and air, at either side of the membrane revealed the presence of bulk diffusional limitations. Oxygen vacancy diffusion coefficients in the range 5.3 to $9.3 \times 10^{-6} \text{ cm}^2 \text{ s}^{-1}$ were calculated from a modified form of Equation (20).

Recently the $\text{La}_{0.4}\text{Ca}_{0.6}\text{Co}_x\text{Fe}_{1-x}\text{O}_{3-\delta}$ ($x = 0, 0.25, 0.5$) series was fabricated and tested in disk form for oxygen permeation and stability studies.³⁷ The study highlighted the difficulties in obtaining a material with good oxygen flux while at the same time possessing long term chemical stability and mechanical strength; the properties that give one benefit can have a deleterious effect on the other resulting in the search for a compromise material. A model assuming bulk diffusion to be rate-determining proved inadequate and was used as indirect evidence for surface exchange limitations for a membrane thickness in the 0.72 to 1.73 mm range. The perovskite with highest cobalt content was mechanically the weakest during long term testing. Reported fluxes were in the range 0.04 to $0.09 \mu\text{mol cm}^{-2} \text{ s}^{-1}$ at 900 °C using argon and air at either side of the disk. Further experiments in which hydrogen was added to the argon side gave an initial flux of $0.83 \mu\text{mol cm}^{-2} \text{ s}^{-1}$ that later stabilised to $0.6 \mu\text{mol cm}^{-2} \text{ s}^{-1}$. Overall permeation activation energies from 84 to 120 kJ mol^{-1} were calculated.

LaGaO_3 , when doped with strontium and magnesium, produces a family that also possesses good oxide anion conductivity. Ishihara *et al.*³⁸ investigated doping cobalt at the gallium-sites in the $\text{La}_{0.8}\text{Sr}_{0.2}\text{Ga}_{0.8}\text{Mg}_{0.2-x}\text{Co}_x\text{O}_{3-\delta}$ system and found an increase in oxide-ion and electronic conductivity. Their work focused on the most promising composition, $\text{La}_{0.8}\text{Sr}_{0.2}\text{Ga}_{0.8}\text{Mg}_{0.115}\text{Co}_{0.085}\text{O}_{3-\delta}$, using electrical conductivity methods, AC IS and ^{18}O exchange on disk samples. This composition gave good oxide-ion conductivity at low temperatures. Values for the oxygen self diffusion coefficient ($4.2 \times 10^{-7} \text{ cm}^2 \text{ s}^{-1}$) obtained from SIMS agreed well with values obtained from conductivity results at 755 °C (such experiments would give a tracer diffusion coefficient; the authors did not state the value of the Haven ratio that was used to convert between the tracer and the self diffusion coefficients). The surface exchange coefficient at this temperature was determined to be $7.9 \times 10^{-7} \text{ cm s}^{-1}$ but it was not clear on which driving force this was based. If a solid-state concentration driving force has been used, these values of surface exchange coefficient would be significantly lower than other values in the literature.^{31,34} This may at least in part be due to the lower temperature but the specific surface condition of the sample would also greatly influence the measured value. Oxygen permeation fluxes of *ca.* $0.16 \mu\text{mol cm}^{-2} \text{ s}^{-1}$ to *ca.* $0.6 \mu\text{mol cm}^{-2} \text{ s}^{-1}$ were observed over the temperature range 600 °C to 1000 °C using dry nitrogen and air at either side of disks of thickness 1.5 mm. Higher cobalt content (x greater than or equal to 0.1) was found to impart good electrical conductivity to this family of solid oxides. A minor increase in phase stability was obtained when nickel was used as the dopant instead of cobalt in the $\text{La}_{0.90}\text{Sr}_{0.10}\text{Ga}_{0.65}\text{Mg}_{0.15}\text{Ni}_{0.2}\text{O}_{3-\delta}$ and $\text{La}_{0.5}\text{Pr}_{0.5}\text{Ga}_{0.65}\text{Mg}_{0.15}\text{Ni}_{0.2}\text{O}_{3-\delta}$ systems at low oxygen partial pressures but praseodymium had a larger positive influence on the stability.³⁹

The Sr-Co-Fe perovskite systems have attracted attention

because they demonstrate the highest oxygen permeabilities of all MIECs but can suffer from degradation in oxygen permeation performance. This is a result of an order–disorder phase transition in the oxygen sublattice from the formation of a brownmillerite phase. Experimental and modelling work concerning the transport mechanism of oxygen in $\text{SrCo}_{0.8}\text{Fe}_{0.2}\text{O}_{3-\delta}$, and for comparison $\text{SmCo}_{0.5}\text{Fe}_{0.5}\text{O}_{3-\delta}$, was undertaken from data collected using tubular membranes.⁴⁰ The oxygen was supplied to the shell side of the membrane tube and varied from 0.01 to 1 atm while helium was supplied to the tube side and contained from 0.002 to 0.07 atm of oxygen. Between 797 and 890 °C the oxygen diffusion coefficient varied from 2.1 to $3.0 \times 10^{-6} \text{ cm}^2 \text{ s}^{-1}$ and the surface exchange coefficient (based on a chemical potential driving force and so not directly comparable with previously cited surface exchange coefficients without the use of an appropriate thermodynamic factor) varied from 3.6 to $9.2 \times 10^{-5} \text{ cm s}^{-1}$ for the $\text{SrCo}_{0.8}\text{Fe}_{0.2}\text{O}_{3-\delta}$ tube of thickness 2.5 mm (inner diameter 3 mm and outer 5.5 mm) and length 9.3 mm. For the larger tube of thickness 2 mm (inner diameter 4.1 mm and outer 6.1 mm) and length 19.2 mm, over the same temperature range, the values for the oxygen diffusion coefficient were found to be larger, varying from 4.0 to $9.3 \times 10^{-6} \text{ cm}^2 \text{ s}^{-1}$ and, for the surface exchange coefficient, from 0.9 to $2.1 \times 10^{-4} \text{ cm s}^{-1}$. The differences in the values of the oxygen diffusion coefficient and the surface exchange coefficient obtained with these two tubes were not discussed. The $\text{SmCo}_{0.5}\text{Fe}_{0.5}\text{O}_{3-\delta}$ tube of thickness 2.8 mm (inner diameter 3.6 mm and outer 6.4 mm) and length 14.8 mm, over the temperature range 800 to 937 °C, gave values for the oxygen diffusion coefficient from 0.21 to $1.25 \times 10^{-6} \text{ cm}^2 \text{ s}^{-1}$ and values for the surface exchange coefficient from 2.5 to $7.5 \times 10^{-5} \text{ cm s}^{-1}$. Although the oxygen diffusion coefficients in these materials were very high relative to other studies, the vacancy diffusion coefficients were similar as a result of the high degree of non-stoichiometry.

The ionic and electronic conductivities of $\text{Sr}_{0.25}\text{Bi}_{0.5}\text{FeO}_{3-\delta}$ were studied by Lu and Liu using AC impedance spectroscopy.⁴¹ Oxygen permeation studies on disk samples of thicknesses 0.4 to 1 mm in the temperature range 700 to 800 °C were also performed using argon and oxygen atmospheres of 0.01, 0.05 and 0.21 atm in nitrogen at either side of the membrane. They found that interfacial resistances limited the oxygen permeation rates under low oxygen partial pressures.

Yang *et al.*⁴² have recently produced two promising new series of $\text{SrCo}_{0.4}\text{Fe}_{0.6-x}\text{Zr}_x\text{O}_{3-\delta}$ ($0 \leq x \leq 0.2$) and $\text{SrCo}_{0.95-x}\text{Fe}_x\text{Zr}_{0.05}\text{O}_{3-\delta}$ ($0.1 \leq x \leq 0.8$) zirconia-containing perovskite materials in an attempt to solve the instability problems in the Sr–Co–Fe perovskite membranes under large oxygen chemical potential differences. Disk membranes of thickness 1.78 mm were used in their permeation study with helium (containing from 0.004 to 0.01 atm of oxygen) and air at either side of the membrane. For the $\text{SrCo}_{0.4}\text{Fe}_{0.6-x}\text{Zr}_x\text{O}_{3-\delta}$ series it was found that 5 mol% of zirconia was sufficient to impart structural stability by reducing oxygen loss from the lattice but without adversely affecting the oxygen flux, high cobalt content in the second family gave rise to oxygen fluxes of $1.37 \mu\text{mol cm}^{-2} \text{ s}^{-1}$ at 950 °C with 5 mol% of zirconia.

The oxygen permeation properties of a novel B-site bismuth-doped perovskite family, $\text{BaBi}_x\text{Co}_{0.2}\text{Fe}_{0.8-x}\text{O}_{3-\delta}$ ($0.1 \leq x \leq 0.5$), was recently investigated by Shao *et al.*⁴³ The oxygen flux was measured using helium and air at either side of a disk membrane. The flux increased with increasing bismuth content at high temperatures (at 950 °C a value of $1 \text{ ml cm}^{-2} \text{ min}^{-1}$ was obtained) apart from when $x = 0.3$ which gave the lowest flux. Increasing the membrane thickness (from 0.66 mm to 1.5 mm) had no effect on oxygen permeation rates at low temperature (600 to 700 °C) whereas, at higher temperatures (700 to 950 °C), the permeation rate was reduced. This was used to suggest that, at low temperature, permeation was controlled by surface

exchange whereas at elevated temperature bulk diffusion became more important.

It has been reported that using barium instead of lanthanum at the A site can improve phase stability of the perovskite by preventing oxidation of the B site cation without adversely affecting oxygen permeability. Shao *et al.*⁴⁴ and Wang *et al.*⁴⁵ prepared $\text{Ba}_{0.5}\text{Sr}_{0.5}\text{Co}_{0.8}\text{Fe}_{0.2}\text{O}_{3-\delta}$ (BSCF5582) in disk and tubular membrane form respectively for oxygen permeation studies. The disk membrane, of thickness 1.8 mm, was operated with helium on one side and an oxygen partial pressure varying between 0.01 and 1 atm on the other side with nitrogen as the balance. The membrane was very stable at temperatures in excess of 850 °C and gave an impressive oxygen flux of $1.4 \text{ ml cm}^{-2} \text{ min}^{-1}$ at 950 °C with an oxygen partial pressure of 0.21 atm on one side and 0.037 atm on the He side (it was not clear if this He-side oxygen was solely a result of oxygen permeation or was controlled in some way). An increase in flux was observed with increasing oxygen partial pressure on the oxygen side and increasing temperature. An overall activation energy for oxygen transport of 40.9 kJ mol^{-1} was calculated. At low oxygen partial pressures and lower temperatures there was evidence of decomposition to different phases; BaCoO_2 was detected by XRD. However, the phase change was found to be reversible with an increase in temperature. In tubular form (outer diameter *ca.* 8 mm, inner diameter *ca.* 5 mm and length up to 300 mm), with wall thickness *ca.* 3 mm, the observed long term oxygen flux at 875 °C was $1.12 \text{ ml cm}^{-2} \text{ min}^{-1}$ using helium and air at the tube and shell side respectively. This steady flow was maintained over a working period of 150 h. The highest flux ($3 \text{ ml cm}^{-2} \text{ min}^{-1}$) was obtained at 900 °C with an oxygen partial pressure of 1 atm on the shell side though the duration of this experiment was not provided. Encouragingly, the material also gave an oxygen vacancy diffusion coefficient of $2.8 \times 10^{-5} \text{ cm}^2 \text{ s}^{-1}$ at 900 °C, similar to that of $\text{SrCo}_{0.8}\text{Fe}_{0.2}\text{O}_{3-\delta}$ ($5.1 \times 10^{-5} \text{ cm}^2 \text{ s}^{-1}$ at 890 °C²⁹) with the advantage of chemical stability in lower partial pressures of oxygen. Data on the degree of non-stoichiometry revealed that δ had a value between 0.258 and 0.316 over this temperature range (700 to 900 °C). These particularly large oxygen deficiencies might be expected to result in instability, but no such instability was reported by the authors.

A dual phase disk membrane containing both $\text{La}_{0.15}\text{Sr}_{0.85}\text{Ga}_{0.3}\text{Fe}_{0.7}\text{O}_{3-\delta}$ and $\text{Ba}_{0.5}\text{Sr}_{0.5}\text{Co}_{0.8}\text{Fe}_{0.2}\text{O}_{3-\delta}$ (LSGF-BSCF with a volume ratio of 1:12.8 prepared by physical mixing and sintering) was recently prepared by Wang *et al.*⁴⁶ This interesting membrane material is composed of dense particles of LSGF separated by a film of the BSCF perovskite. The two mixed phases were initially sintered to a temperature between the melting points of the LSGF and BSCF causing the LSGF to form large grains with grain boundaries. The BSCF became molten and slowly covered the LSGF grains forming a film running through the grain boundaries of the LSGF phase. This system gave an oxygen permeation flux of $0.45 \text{ ml cm}^{-2} \text{ min}^{-1}$ at 915 °C using helium and dry air on either side of a membrane disk of thickness 2 mm. This flux was much higher than that which was obtained with a LSGF membrane alone ($0.05 \text{ ml cm}^{-2} \text{ min}^{-1}$) while the LSGF-BSCF membrane was more stable than BSCF alone in reducing hydrogen atmospheres. Oxygen permeation on membranes of thickness 1.5 mm to 2 mm over the temperature range 800 to 900 °C indicated bulk diffusion was the limiting step. The reported duty time of the system was 120 h at 850 °C and 180 h at 900 °C during which time the oxygen permeation flux was stable.

4. Applications of MIEC membranes to chemical production

Appreciable oxygen fluxes are only obtained at relatively high temperatures in MIEC membrane systems. This means that

any application of these membranes is only suited to the activation of highly stable reactant molecules and, in practice, has meant most work has been performed on the reactions of methane. The methane molecule has a high C–H bond strength and in general is the least reactive alkane; it has a very high ionisation energy and decomposes into free C and H at a temperature of 785 °C. (A review of the properties and chemistry of methane has been provided by Crabtree.⁴⁷) Membrane reactors show promise for improved yields for methane partial oxidation processes as the methane feed is not mixed with gas-phase oxygen which may reduce the possibility of the total oxidation of the methane and any partial oxidation reaction products. When employing MIECs in membrane reactors it must of course be remembered that in addition to high oxygen fluxes it is also beneficial if the surface of the membrane possesses catalytic activity for the desired reaction or, alternatively, the membrane tube should be packed with a conventional catalyst. In summarising recent work we indicate for each reference whether the reactor was packed with catalyst, the membrane surface was catalytically modified or the membrane surface was left unmodified.

This section is focussed on recent studies concerned with the production of syngas (carbon monoxide and hydrogen), from methane and air. However it is perhaps worthwhile briefly mentioning the oxidative coupling of methane (OCM), though the application of MIEC membranes to this process has only attracted a fraction of the interest that has been given to syngas production. The OCM process promises the direct conversion of methane into higher hydrocarbons in a single step and as such is a highly desirable process. Selectivity to C₂ products, *i.e.*, ethane and ethene, for OCM are most favourable at low oxygen partial pressures. This can be achieved by the distribution of oxygen injection ports along the length of a reactor. This system can be greatly simplified by use of a membrane reactor in which the entire surface can provide, in effect, an infinite number of injection ports to give significant yields with high selectivity by minimising undesirable complete oxidation. MIEC membranes recently applied to OCM have mainly been of the LSCF family namely, LSCF6482,^{48,49} 8264,⁵⁰ 6428^{51,52} and 4628.⁵² However other perovskite membranes tested have included La_{0.8}Ba_{0.2}Co_{0.8}Fe_{0.2}O_{3-δ},⁴⁸ La_{0.2}Ba_{0.8}Co_{0.2}Fe_{0.8}O_{3-δ},⁵² BSCF5582,⁵³ and BaCe_{0.8}Gd_{0.2}O_{3-δ}.⁵⁴ Performance has been hampered by stability of the membrane as a result of the large oxygen chemical potential difference when exposed to reducing conditions leading to failure of the membrane. Selectivity to C₂s as high as 70%, with conversions of the order of 1 to 3%, at 800 °C have been reported by ten Elshof *et al.*^{48,49} while Zeng *et al.*⁵⁰ have reported C₂ selectivity in the range 70 to 90% with conversions of 10 to 18% at temperatures higher than 850 °C. However, with increasing methane content in the feed, selectivity to C₂s reduced to less than 40%. In general, progress in improving the OCM process using MIEC membranes has not been rapid and results indicate that more investigations need to be performed to improve yields and membrane stability. Reviews dealing with the use of membrane technology for other reactions and current problems with such technology have been reviewed elsewhere.^{24–26,55}

In spite of fundamental difficulties in activating the methane molecule, dwindling oil reserves has caused attention to turn to natural gas (composed primarily of methane) as a source of starting material for the manufacture of industrially important chemicals. Most commonly the first step in this process is the conversion of the raw methane into syngas (hydrogen and carbon monoxide) *via* the endothermic steam reforming process,



The conventional energy intensive steam reforming method is

operated at pressures of the order of 15 to 30 atm at 850 to 900 °C. An alternative is to use an MIEC membrane for the modestly exothermic partial oxidation of methane,



The syngas can then be upgraded in a second step to value-added higher hydrocarbons by the Fischer–Tropsch process or converted to methanol. An MIEC membrane is particularly attractive in this application as air can be used as the oxidant with no mixing of nitrogen with the product stream. An additional benefit concerns safety, with the methane and oxygen sources effectively isolated, the chances of explosive mixtures occurring is greatly diminished. In Table 1 we list the complex perovskites that have recently been investigated for the application of syngas production using small laboratory-scale test reactors.

The LSCF perovskite membranes have been investigated in recent studies for syngas production. Jin *et al.*^{56,57} have studied the performance of a tubular LSCF6428 membrane (outer diameter 8 mm, wall thickness 1.5 mm and length 150 mm) packed with a Ni/γ-Al₂O₃ catalyst in the temperature range 825 to 885 °C. Dilute methane and air were used on either side of the tubes. At low methane mole fractions in the feed, in the temperature range 825 °C to 885 °C, excellent conversion (>96%) and selectivity to CO (>97%) was reported. At methane mole fractions greater than 6% the conversion decreased and coke was formed. However after only a few hours of operation (3 to 7 h) using 6% methane in helium, mechanical failure of the membrane occurred because of the reduction of metal cations that then segregated to the membrane surface. Such mechanical failure, caused by exposure to reducing atmospheres, is a recurring problem in studies of this type and is a result of a volumetric lattice mismatch between the inner and outer membrane walls arising from the difference in oxygen chemical potential across the membrane. Wachsmann and Clites⁵⁸ addressed the problem of mechanical failure by using a bi-layered membrane composed of a thin film of (Sm₂O₃)_{0.1}(CeO₂)_{0.9} (SDC), of thickness 0.1 to 0.3 μm, deposited on the reducing side of a 2 mm thick LSCF6482 disk membrane. Dilute methane and synthetic air were used on either side of the disk. An oxygen flux of 0.44 ml (STP) cm⁻² min⁻¹ (0.33 μmol cm⁻² s⁻¹) was maintained for 50 h of operation, the condition of the membrane was not commented upon after this period of operation. The SDC layer acts as a protective layer for the LSCF membrane by shielding it from the critical partial pressure of oxygen at which the ceramic becomes unstable. An interesting observation reported in the paper was the oscillatory behaviour in the production of carbon monoxide, and the corresponding conversion of methane, as a result of a reduction/oxidation cycle of ceria in the SDC layer with a period of *ca.* 2 h. Tubular membranes of LSCF2882 (outer diameter 6.5 mm, wall thickness 0.5 to 1.2 mm and length *ca.* 300 mm) have been fabricated by the plastic extrusion method and tested at 850 °C using 80% methane with 20% argon on the shell side and air on the tube side with a rhodium-based reforming catalyst, the exact nature of which was not specified.⁵⁹ The material was found to be brittle under operating conditions, breaking in a matter of minutes. *In situ* XRD studies at a low partial pressure of oxygen of 0.05 atm revealed transformation of the perovskite to an oxygen-vacancy-ordered phase with the oxide expanding significantly following this phase change. The understanding of mechanical failure in La_{0.2}Sr_{0.8}Cr_{0.2}Fe_{0.8}O_{3-δ} has been the goal of recent work by Majkic *et al.*^{60,61} Both oxygen partial pressures and the grain size were found to play a role in the creep behaviour. Detailed fracture characterisation of tubular La_{0.2}Sr_{0.8}Cr_{0.2}Fe_{0.8}O_{3-δ} membranes carried out by Nagendra *et al.*^{62,63} showed significant loss of strength in even mildly

reducing conditions with transgranular cleavage and secondary phases forming. A brownmillerite secondary phase was responsible for a lattice expansion causing additional stress.

In a study by Balachandran *et al.*,⁶⁴ membrane tubes of $\text{SrCo}_{0.8}\text{Fe}_{0.2}\text{O}_{3-\delta}$ (outer diameter 6.5 mm, wall thickness 0.5 to 1.2 mm and length *ca.* 300 mm) were tested using, on the shell side, 80% methane with 20% argon and air on the tube side with a rhodium-based reforming catalyst (the exact chemical nature and physical form of this catalyst were not specified by the authors). The membrane proved to be disappointing in operation, lasting only a few minutes due to severe lattice expansion leading to cracking. This structural instability was observed prior to reaction conditions by high-temperature XRD in the presence of 0.01 atm of O_2 at 850 °C. Structural oxygen was lost and new phases developed. In comparison, a non-perovskite material $\text{SrCo}_{0.5}\text{Fe}_{0.5}\text{O}_{3-\delta}$ proved to be much superior, withstanding 1000 h of duty time. A tubular membrane reactor of YSZ-promoted $\text{SrCo}_{0.4}\text{Fe}_{0.6}\text{O}_{3-\delta}$ (outer diameter 7.7 mm, wall thickness 3.6 mm and length *ca.* 300 mm) has been investigated.⁶⁵ Oxygen permeation studies at 850 °C using helium and air gave a steady flux of 0.19 ml (STP) $\text{cm}^{-2} \text{min}^{-1}$ (0.14 $\mu\text{mol cm}^{-2} \text{s}^{-1}$) over a period of 110 h. The tube was then loaded with a Ni/ γ - Al_2O_3 catalyst and operated under reaction conditions at 850 °C with methane diluted in helium at the tube side and air at the shell side. The membrane failed after 4 h of operation but with a small amount of oxygen added to the methane feed (around 5% of that permeating through the membrane tube) performance was maintained for over 70 h as membrane decomposition was retarded. The oxygen flux under these reaction conditions stabilised at 4.6 ml (STP) $\text{cm}^{-2} \text{min}^{-1}$ (3.4 $\mu\text{mol cm}^{-2} \text{s}^{-1}$) towards the end of the period of operation. This was believed to be as a result of replenishment of lattice oxygen consumed at the inlet of the membrane tube. Conversion of methane was 100% over this period with an initial CO selectivity of 62% rising to 82% over the first 35 h and then declining again to *ca.* 55% towards the end of the 70 h operating time. No mention was made of the fate of the missing carbon.

Doped LaGaO_3 perovskites, $\text{La}_{0.7}\text{Sr}_{0.3}\text{Ga}_{0.6}\text{Fe}_{0.4}\text{O}_{3-\delta}$ ⁶⁶ and $\text{La}_{0.8}\text{Sr}_{0.2}\text{Ga}_{0.7}\text{M}_{0.3}\text{O}_{3-\delta}$ ⁶⁷ (M = Fe, Co, Ni) have been investigated by Ishihara *et al.* A $\text{La}_{0.7}\text{Sr}_{0.3}\text{Ga}_{0.6}\text{Fe}_{0.4}\text{O}_{3-\delta}$ ⁶⁶ disk of thickness 0.5 mm was coated with a 40 μm layer of $\text{La}_{0.6}\text{Sr}_{0.4}\text{CoO}_3$ on the oxygen reduction side of the disk. Oxygen permeation rates from 0.5 to 0.8 ml (STP) $\text{cm}^{-2} \text{min}^{-1}$ (0.37 to 1.3 $\mu\text{mol cm}^{-2} \text{s}^{-1}$) was obtained between 600 and 1000 °C using air and helium on either side of the membrane. Varying the membrane thickness (0.3 mm to 1 mm) indicated bulk diffusion was rate determining. For syngas production, various catalysts, nickel, palladium, ruthenium, rhodium, cobalt and iron were applied on the methane side of the disk membrane. This was performed by screen-printing *ca.* 30 mg of either the oxide or chloride onto the membrane to give a coating of *ca.* 40 μm thickness and then reducing in hydrogen at 1000 °C to obtain the active metal. Methane was supplied to one side of the disk diluted in nitrogen (in a 2:1 ratio) and dry air was supplied to the other. Modification of the membrane surface with nickel and ruthenium gave the best performance. An oxygen permeation rate of 8 ml (STP) $\text{cm}^{-2} \text{min}^{-1}$ (5.4 $\mu\text{mol cm}^{-2} \text{s}^{-1}$) at 1000 °C with a membrane thickness of 0.5 mm was recorded with the nickel catalyst under reaction conditions. Nickel gave the best yield of syngas (37%) at 37% conversion, implying the absence of any competing reaction and, indeed, no coke formation was observed. In the case of a nickel catalyst, the authors did not observe, by XRD or SEM, any degradation of the membrane. Cobalt gave the poorest yield of syngas (7%), still with high selectivity. It was found that nickel-doping of the $\text{La}_{0.8}\text{Sr}_{0.2}\text{Ga}_{0.7}\text{M}_{0.3}\text{O}_{3-\delta}$ ⁶⁷ system gave the highest oxygen flux in experiments using nitrogen and air on either side of a membrane disk of thickness 0.5 mm in the

temperature range 750 to 1000 °C. The flux varied from 0.25 $\mu\text{mol cm}^{-2} \text{s}^{-1}$ at *ca.* 750 °C to *ca.* 1 $\mu\text{mol cm}^{-2} \text{s}^{-1}$ at 1000 °C. Of all the dopants tested, iron gave the best stability when exposed to the reducing methane atmosphere and further tests indicated that oxygen permeation increased with increasing iron content. In this work, nickel was used as a reforming catalyst⁶⁷ though the quantity and method of application were not stated. In a comparison study with the widely investigated LSCF6428 the $\text{La}_{0.7}\text{Sr}_{0.3}\text{Ga}_{0.6}\text{Fe}_{0.4}\text{O}_{3-\delta}$ system gave consistently higher methane conversions from *ca.* 5% to *ca.* 40% (compared to *ca.* 5% to *ca.* 25% for LSCF6428) over the temperature range 750 to 1000 °C. The authors observed a 2:1 ratio of hydrogen to carbon monoxide, with only trace amounts of carbon dioxide, while no coke was observed implying virtually 100% selectivity although the selectivity was not explicitly stated.

Tubular⁶⁸ (outer diameter *ca.* 8 mm, wall thickness *ca.* 3 mm and length *ca.* 300 mm) and disk^{53,69,70} membranes of BSCF558 have been investigated with some impressive results. High stability of the tubular membranes over long operating periods, of the order of 500 h, with selectivities to hydrogen and carbon monoxide of *ca.* 95% and conversion of 94% at 875 °C were reported with $\text{LiLaNiO}_x/\gamma\text{-Al}_2\text{O}_3$ catalyst particles of mesh size 40–60 (0.24–0.42 mm) used as a reforming catalyst. Under reaction conditions, using 80% methane in helium and air in the shell and tube side respectively, the tubular membrane gave an oxygen flux of *ca.* 6 to 12 ml $\text{cm}^{-2} \text{min}^{-1}$ over the temperature range 825 to 925 °C. The oxygen permeation flux was found to depend on the flow rate of the air to the shell side, indicating mass transfer limitations. This was overcome by increasing the airflow rate. The trends in the oxygen permeation, product selectivity and methane conversion indicated that the reaction followed a combustion and reforming mechanism. This involves a two-step process by which methane is converted firstly by complete combustion to carbon dioxide and water followed by reforming of any excess methane by the steam and carbon dioxide created in the first step.

5. Summary and future direction

Mixed ionic and electronic conductors (MIECs) exhibit both appreciable ionic conductivity and electronic conductivity. This means that MIECs cannot be used for the direct external electrical control of the flux of a species to a catalyst surface nor can they be effectively employed in fuel cells as electrolyte materials. This limits their application to simultaneous reaction and separation problems. When used as a membrane, the MIEC essentially acts as a barrier between two chambers and only the ionically-conducted species can pass through the membrane under a chemical potential gradient. Here we have focussed on the applications of oxygen-ion conducting MIEC membranes in chemical production. Such membranes promise advantages when used for oxidation processes as air can be used as an oxidant with no mixing of nitrogen with the product stream.

Application has been limited to high temperature processes because of the need for good membrane conductivities. The vast majority of work in this area has been devoted to application for syngas production and to a lesser extent for the oxidative coupling of methane. Central to their use is the long-term stable oxygen flux that can be delivered without adversely effecting membrane stability. The La–Sr–Co–Fe system has received the most attention but promise has also been shown by the Sr–Co–Fe and Ba–Sr–Co–Fe systems, the latter in particular has demonstrated particular robustness in long-term operation under laboratory scale testing. However only a few studies have provided fluxes approaching the desirable range of 1 to 10 ml $\text{cm}^{-2} \text{min}^{-1}$ and this only at elevated temperatures of *ca.* 900 °C. Any greater fluxes, up to 12 ml $\text{cm}^{-2} \text{min}^{-1}$

(for BSCF5582), reported have been under reaction conditions in which very large oxygen chemical potential gradients are established; such gradients simultaneously causing membrane failure.

The challenge in all membrane systems is to improve both membrane fluxes and stability; MIEC membranes are no exception. Future work will undoubtedly involve improving the conductivity of MIECs through better understanding of material properties and better consequent material selection. Such improvements in conductivity will allow the temperature of operation of the membrane systems to be reduced, in turn allowing the application of the membranes to other reaction systems. In addition better techniques for membrane fabrication, providing strong, durable membranes with only thin dense layers incorporated, will also improve overall membrane fluxes. Work in the area of catalytic modification of the membrane surface itself (an area that has to date received little attention) also promises to yield higher membrane fluxes under reaction conditions. The improvement of membrane stability, and the balance between decreased stability and increased flux, deserves further attention and will be critical to successful commercial exploitation. Further work must also include obtaining a better understanding of processes at the membrane surface, the effect of grain-boundaries on conductivity, and order-disorder events of the crystal structure.

Acknowledgements

The authors wish to thank Dr Kang Li of the Department of Chemical Engineering, Imperial College, for supplying Fig. 3.

References

- P. J. Jellings and H. J. M. Bouwmeester, *Catal. Today*, 1992, **12**, 1.
- S. Wang, Y. Zang, W. Li, J. Yan, Z. Lu and G. A. Tompsett, *Solid State Ionics*, 1999, **120**, 75.
- I. Reiss, *Solid State Ionics*, 2003, **157**, 1.
- S. Primdahl and M. Mogensen, *Solid State Ionics*, 2002, **152-153**, 597.
- B. C. H. Steele, *Mater. Sci. Eng.*, 1992, **B13**, 79.
- H. J. M. Bouwmeester, *Catal. Today*, 2003, **82**, 141.
- J. C. Boivin and G. Mairesse, *Chem. Mater.*, 1998, **10**, 2870.
- J. Kohler, N. Imanaka and G.-y. Adachi, *Chem. Mater.*, 1998, **10**, 3790.
- J.-C. Boivin, *Int. J. Inorg. Mater.*, 2001, **3**, 1261.
- D. M. Smyth, *Solid State Ionics*, 2000, **129**, 5.
- M. Mogensen, N. M. Sammes and G. A. Tompsett, *Solid State Ionics*, 2000, **129**, 63.
- J. Schoonman, in *Solid State Electrochemistry*, ed. P. J. Gellings and H. J. M. Bouwmeester, CRC Press, New York, 1997, p. 161.
- P. Kofstad, *Nonstoichiometry, diffusion and electrical conductivity in binary metal oxides*, Wiley, New York, 1972.
- P. Cousin and R. A. Ross, *Mater. Sci. Eng.*, 1990, **A130**, 119.
- K. C. Patel, S. T. Aruna and T. Mimani, *Curr. Opin. Solid State Mater. Sci.*, 2002, **6**, 507.
- D. Brinkmann, *Magn. Reson. Rev.*, 1989, **14**, 101.
- Characterisation of ceramics*, ed. L. L. Hench and R. W. Gould, Marcel Dekker Inc., New York, 1971.
- P. J. E. Flewitt and R. K. Wild, *Grain Boundaries: Their microstructure and Chemistry*, Wiley, New York, 2001.
- M. Trunec, *J. Eur. Ceram. Soc.*, 2003, **24**, 645.
- X. Tan, S. Liu and K. Li, *J. Membr. Sci.*, 2001, **188**, 87.
- S. Liu, X. Tan, K. Li and R. Hughes, *J. Membr. Sci.*, 2001, **193**, 249.
- S. Liu, K. Li and R. Hughes, *Mater. Res. Bull.*, 2004, **39**, 119.
- J. Luyten, A. Buekenhoudt, W. Adriansens, J. Cooymans, H. Weyten, F. Servaes and R. Leysen, *Solid State Ionics*, 2000, **135**, 637.
- J. Zaman and A. Chakma, *J. Membr. Sci.*, 1994, **92**, 1.
- M. Stoukides, *Catal. Rev. Sci. Eng.*, 2000, **42**(1&2), 1.
- S.-T. Hwang, *Korean J. Chem. Eng.*, 2001, **18**(6), 775.
- R. J. Chater, S. Carter, J. A. Kilner and B. C. H. Steele, *Solid State Ionics*, 1992, **53-56**, 85.
- J. A. Lane, S. J. Benson, D. Waller and J. A. Kilner, *Solid State Ionics*, 1999, **121**, 201.
- S. Li, H. Qi, N. Xu and J. Shi, *Ind. Eng. Res.*, 1999, **38**, 5028.
- W. Jin, S. Li, P. Huang, N. Xu and J. Shi, *J. Membr. Sci.*, 2001, **185**, 273.
- S. Diethelm and J. Van herle, *J. Eur. Ceram. Soc.*, 2004, **24**, 1319.
- S. Li, W. Jin, P. Huang, N. Xu, J. Shi, Y. S. Lin, M. Z.-C. Hu and E. A. Payzant, *Ind. Eng. Res.*, 1999, **38**, 2963.
- Y. Teraoka, Y. Hombe, J. Ishii, H. Furukawa and I. Moriguchi, *Solid State Ionics*, 2002, **152-153**, 681.
- J. E. ten Elshof, M. H. R. Lankhorst and H. J. M. Bouwmeester, *Solid State Ionics*, 1997, **99**, 15.
- Z. Yang, Y. S. Lin and Y. Zeng, *Ind. Eng. Res.*, 2002, **41**, 2775.
- J. E. ten Elshof, J. M. Bouwmeester and H. Verweij, Part I, *Solid State Ionics*, 1995, **81**, 97; J. E. ten Elshof, J. M. Bouwmeester and H. Verweij, Part II, *Solid State Ionics*, 1996, **89**, 81.
- S. Diethelm, J. Van herle, P. H. Middleton and D. Favrat, *J. Power Sources*, 2003, **118**, 270.
- T. Ishihara, H. Furutani, M. Honda, T. Yamada, T. Shibayama, T. Akbay, N. Sakai, H. Yokokawa and Y. Takita, *Chem. Mater.*, 1999, **11**, 2081.
- V. V. Kharton, A. A. Yaremchenko, A. L. Shaula, M. V. Patrakeev, E. N. Naumovich, D. I. Logvinovich, J. R. Frade and F. M. B. Marques, *J. Solid State Chem.*, 2004, **177**, 26.
- S. Kim, Y. L. Yang, A. J. Jacobson and B. Abeles, *Solid State Ionics*, 1998, **106**, 189.
- X. Lu and M. Liu, *Solid State Ionics*, 2002, **149**, 299.
- L. Yang, L. Tan, X. Gu, W. Jin, L. Zhang and N. Xu, *Ind. Eng. Res.*, 2003, **42**, 2299.
- Z. Shao, G. Xiong, Y. Cong and W. Yang, *J. Membr. Sci.*, 2000, **164**, 167.
- Z. Shao, W. Yang, Y. Cong, H. Dong, J. Tong and G. Xiong, *J. Membr. Sci.*, 2000, **172**, 177.
- H. Wang, Y. Cong and W. Yang, *J. Membr. Sci.*, 2002, **210**, 259.
- H. Wang, W. S. Yang, Y. Cong, X. Zhu and Y. S. Lin, *J. Membr. Sci.*, 2003, **224**, 107.
- R. H. Crabtree, *Chem. Rev.*, 1995, **95**, 987.
- J. E. ten Elshof, B. A. Vanhassel and H. J. M. Bouwmeester, *Catal. Today*, 1995, **25**, 397.
- J. E. ten Elshof, H. J. M. Bouwmeester and H. Verweij, *Appl. Catal. A: Gen.*, 1995, **130**, 195.
- Y. Zeng, Y. S. Lin and S. L. Swartz, *J. Membr. Sci.*, 1998, **150**, 87.
- J. S. Xu and W. J. Thomson, *Ind. Eng. Chem. Res.*, 1998, **37**, 1290.
- J. S. Xu and W. J. Thomson, *AIChE J.*, 1997, **43**(11A), 2731.
- Z. Shao, H. Dong, G. Xiong, Y. Cong and W. Yang, *J. Membr. Sci.*, 2001, **183**, 181.
- Y. Lu, A. G. Dixon, W. R. Moster, Y. Ma and U. Balachandran, *Catal. Today*, 2000, **56**, 297.
- G. Saracco, G. F. Versteeg and W. P. M. van Swaaij, *J. Membr. Sci.*, 1994, **95**, 105.
- W. Jin, X. Gu, S. Li, P. Huang, N. Xu and J. Shi, *Chem. Eng. Sci.*, 2000, **55**, 2617.
- W. Jin, S. Li, P. Huang, N. Xu, J. Shi and Y. S. Lin, *J. Membr. Sci.*, 2000, **166**, 13.
- E. D. Wachsman and T. L. Clites, *J. Electrochem. Soc.*, 2002, **149**(3), A424.
- U. Balachandran, J. T. Dusek, R. L. Mieville, R. B. Poeppel, M. S. Kleefisch, S. Pei, T. P. Kobylinski, C. A. Udovich and A. C. Bose, *Appl. Catal. A: Gen.*, 1995, **133**, 19.
- G. Majkic, L. T. Wheeler and K. Salama, *Solid State Ionics*, 2002, **146**, 393.
- G. Majkic, L. T. Wheeler and K. Salama, *Solid State Ionics*, 2003, **164**, 137.
- N. Nagendra, R. F. Klie, N. D. Browning and S. Bandhopadhyay, *Mater. Sci. Eng.*, 2003, **A341**, 236.
- N. Nagendra and S. Bandhopadhyay, *J. Eur. Ceram. Soc.*, 2003, **23**, 1361.
- U. Balachandran, J. T. Dusek, P. S. Maiya, B. Ma, R. L. Mieville, R. B. Poeppel, M. S. Kleefisch and C. A. Udovich, *Catal. Today*, 1997, **36**, 265.
- X. Gu, L. Yang, L. Tan, W. Jin, L. Zhang and N. Xu, *Ind. Eng. Res.*, 2003, **42**, 795.
- T. Ishihara, Y. Tsuruta, T. Todaka, H. Nishiguchi and Y. Takita, *Solid State Ionics*, 2002, **152**, 709.
- T. Ishihara, T. Yamada, H. Arikawa, H. Nishiguchi and Y. Takita, *Solid State Ionics*, 2000, **135**, 631.
- H. Wang, Y. Cong and W. Yang, *Catal. Today*, 2003, **82**, 157.
- Z. Shao, G. Xiong, H. Dong, W. Yang and L. Lin, *Sep. Purif. Technol.*, 2001, **25**, 97.
- H. Dong, Z. Shao, G. Xiong, J. Tong, S. Sheng and W. Yang, *Catal. Today*, 2001, **67**, 3.